Photoelastic properties of zinc-blende $Al_xGa_{1-x}N$ in the UV: Picosecond ultrasonic studies

J. Whale, A. V. Akimov,[*] S. V. Novikov, C. J. Mellor, and A. J. Kent

School of Physics and Astronomy, University of Nottingham, University Park, Nottingham NG7 2RD, United Kingdom

Picosecond ultrasonics was used to study the photoelastic properties of zinc-blende (cubic) c-$Al_xGa_{1-x}N$ with x around 0.5. The velocities for longitudinal sound in the alloys were measured using ultrafast UV pump-probe experiments with (AlGa)N membranes. Strong Brillouin oscillations were observed in (AlGa)N films attached to GaAs substrates. These oscillations are due to the dynamical interference of the probe beams reflected from the sample surface and interfaces and a picosecond-duration strain pulse propagating in the alloy layer. Optical and elasto-optical parameters including the complex refractive index and the fundamental band gap of the cubic nitride alloys are determined and compared with the values obtained by ellipsometry.

I. INTRODUCTION

There is a strong demand for efficient deep-UV (<300 nm) semiconductor light sources for various applications, notably water purification [1–3]. The nitride alloy $Al_xGa_{1-x}N$ is a prospective candidate materials system for fabricating such devices. The band gap of $Al_xGa_{1-x}N$ ranges from $E_g = 3.2$ eV (for $x = 0$) to $E_g \approx 6$ eV (for $x = 1$), and its value can be controlled by varying the aluminum content x in the alloy. Most of the optical studies with (AlGa)N alloys have been performed on wurtzite h-$Al_xGa_{1-x}N$ layers epitaxially grown on c-axis sapphire or SiC substrates. These layers possess strong piezoelectric and spontaneous polarization effects which can, in some circumstances, affect the efficiency of optoelectronic device structures [4]. Zinc-blende (cubic) $Al_xGa_{1-x}N$ layers do not exhibit piezoelectric and spontaneous polarization effects [5], which makes c-(AlGa)N attractive for optoelectronic applications. Furthermore, because c-AlGaN can be grown by MBE on Si and GaAs substrates, the optoelectronic devices can be integrated with conventional Si- and GaAs-based electronic devices. However, the cubic phase of AlGaN is metastable and it is difficult to grow high-quality layers containing few stacking faults and a small hexagonal component, therefore there are only a few works where the optical properties of c-$Al_xGa_{1-x}N$ have been studied [6–8]. In those experiments, the ellipsometry technique was used to measure the layer thickness as well as the refractive index and extinction coefficient. This provided information about the electronic band structure and also characterized the quality of the grown layers.

Ellipsometry is a powerful technique, but still possesses some uncertainty in defining the dielectric function of the layers and the thicknesses in the case of multilayered structures, particularly in the UV spectral range where the basic optical properties of some materials are not well known. A technique that can complement ellipsometry is *picosecond ultrasonics* [9], which can measure the same optical parameters (e.g., refractive index and extinction coefficient) and can also obtain the photoelastic properties of the materials; the latter providing a route to the application of high-frequency ultrasonics in UV nanoscopic imaging [10] and ultrafast modulation [11,12] of nitride based lasers and light-emitting diodes. Picosecond ultrasonics was previously used to study the photoelastic properties of h-GaN and related nanostructures [13]. More recently, a few experiments have been carried out on c-GaN layers [14], c-GaN membranes [15], and c-GaN/AlGaN quantum wells [16].

In the present paper, we report the results of the experiments where we use picosecond ultrasonics to measure the photoelastic properties of c-$Al_xGa_{1-x}N$ epilayers with x around 0.5. From the experiments performed on free-standing membranes we obtain the sound velocity s for three layers with different nominal values of x. Measurements of the dynamical interference of the probe light with the picosecond strain pulse (so-called Brillouin oscillations) allow us to derive the complex refractive index, and estimate the photoelastic parameters and their dependencies on probe wavelength. Monitoring the reflection of coherent phonons with frequency ∼100 GHz at the free surface of the c-$Al_xGa_{1-x}N$ layer gives us information regarding the submicrometer roughness of the free surface.

II. EXPERIMENT AND RESULTS

A. Samples and experimental details

We present detailed results for three c-$Al_xGa_{1-x}N$ layers with $x = 0.42$, 0.49, and 0.66. The samples were grown by molecular beam epitaxy (MBE) on semi-insulating (100) GaAs substrates with a c-GaN buffer layer. The AlN fraction was measured by electron probe microanalysis (EPMA) using a Cameca SX100 system [17] and the fractional error for x did not exceed 2%. The thicknesses of the c-$Al_xGa_{1-x}N$ and c-GaN buffer layers were around 300 and 50 nm respectively and the values measured by a J. A. Woollam M-2000 ellipsometer are given in Table I. The uncertainty in the thickness of the

_____

[*]Corresponding author: andrey.akimov@nottingham.ac.uk

TABLE I. Photoelastic parameters of c-Al$_x$Ga$_{1-x}$N measured in the present work and compared with the data obtained earlier. The values obtained from ellipsometry data are in brackets. The accuracy for obtaining n and κ from ellipsometry measurements are ±0.05 and $\pm2.5\%$ respectively.

		c-GaN ($x=0$)	$x=0.42$	$x=0.49$	$x=0.66$	c-AlN ($x=1$)
Thickness of the buffer c-GaN layer (nm)			57 ± 10	49 ± 10	57 ± 10	
Thickness of the alloy layer (nm)			282 ± 12	289 ± 10	286 ± 10	
Density (kg/m^3)		6000	4824	4628	4152	3200[a]
Speed of sound (m/s)	Measured		7940 ± 380	8017 ± 340	8855 ± 290	
	Linear fit	7000[b]	8100	8283	8728	9619[a]
Direct band gap E_g (eV)		3.2[d]	4.4 ± 0.2 (4.47)	4.5 ± 0.2 (4.47)	4.8 ± 0.2 (4.86)	5.93[c,e]
			3.87[d], 4.1[e]	3.98[d], 4.2[e]	4.26[d], 4.5[e]	5.0[d]
Refractive index at $E=E_g$, n		2.8[d]	2.7 ± 0.1 (2.72)	2.6 ± 0.1 (2.63)	2.6 ± 0.1(2.54)	2.9[c]
				2.4 for $x=0.46$[d]		2.3[d]
Extinction at $E=E_g$, κ		0.25[d]	0.05 (0.22)	0.05 (0.16)	0.05 (0.14)	$\sim$0.01[c]
				0.15 for $x=0.46$[d]		0.15[d]
Photoelastic parameters	α		10 at 4.25 eV	2 at 4.3 eV	8 at 4.6 eV	
			-6 at 4.55 eV	-3 at 4.7 eV	-4 at 4.8 eV	
	β		2 at 4.37 eV	1 at 4.5 eV	2 at 4.8	

[a]Reference [20].
[b]References [14,15].
[c]Reference [25].
[d]References [6,7].
[e]Reference [8].

layers was better than ±15 nm. The edge-supported (AlGa)N membranes were fabricated by wet chemical etching of a 1-mm-diameter hole from the back of the GaAs substrate through to the nitride layer. Standard UV photolithographic techniques were used to define the hole.

A detailed description of the picosecond acoustics technique may be found elsewhere [9]. The picosecond ultrasonic experiments were performed using a two color UV optical pump-probe setup, the schematic for which may be found in the Supplemental Material [18]. The laser system included an 82-MHz Ti-sapphire oscillator (wavelength $\lambda_0 = 700$–900 nm, pulse duration 120 fs) and an optical harmonic generator, which had outputs for second and third harmonics with wavelength $\lambda_2 = \lambda_0/2$ and $\lambda_3 = \lambda_0/3$ respectively. The average power of the pump and probe beams were $\sim$10 and $\sim$1 mW respectively and both beams were focused to a spot diameter of $\sim$20 μm on the sample with the pump spot slightly larger than the probe. A beam from one output (pump) with wavelength λ_{pu} was used for generating picosecond strain pulses [9,19] and the beam from the other output (probe) with wavelength λ_{pr} was used to detect the strain pulses. Depending on the experiments, we used either $\lambda_{pr} > \lambda_{pu}$ or $\lambda_{pu} > \lambda_{pr}$. The pump beam was modulated using an acousto-optical modulator at a frequency of 200 kHz and the reflected probe beam was detected by a UV-enhanced silicon photodiode.

B. (AlGa)N membranes

In the experiments with the membranes, we used pump wavelengths of $\lambda_{pu} = \lambda_3 = 258$–$280$ nm, and the probe $\lambda_{pr} = \lambda_2 = 387$–$420$ nm arranged in reflection geometry. The main panel in Fig. 1 shows the pump-probe signals $\Delta R(t)$ as a function of delay time t between pump and probe pulses. After a sharp step, oscillations with frequency $f_m \sim 10$ GHz are clearly observed. These oscillations are due to the fundamental vibrational mode of the membrane. The modes with higher frequency are not observed in our experiments because of their much smaller amplitude which agrees with earlier studies on pure c-GaN membranes [15]. The left inset in Fig. 1 shows the fast Fourier transforms (FFTs) of the oscillations and it is seen that f_m increases with the increase of the Al content.

The measured values of f_m allow us to obtain the velocity s_a of longitudinal acoustic phonons in the c-(AlGa)N alloy. For this we take into consideration a thin c-GaN buffer layer which remains in the membrane after back-etching the GaAs

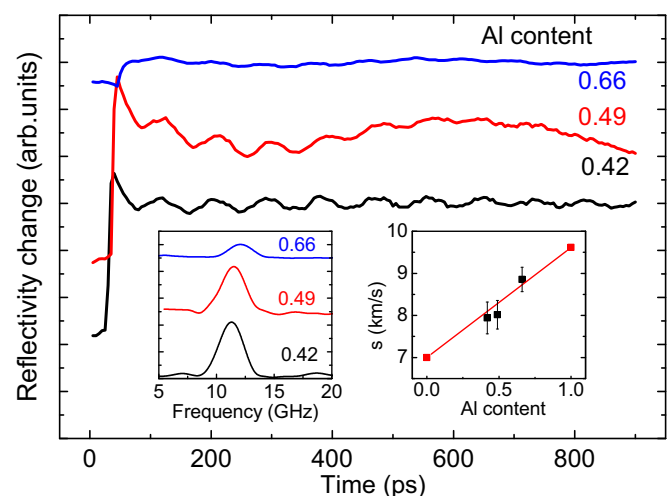FIG. 1. Pump-probe signals measure in c-Al$_x$Ga$_{1-x}$N membranes; left inset: fast Fourier transforms (FFTs) of the background free signals, shown in the main panel; right inset: the sound velocity of the alloy as a function of Al content (black squares) and linear interpolation (red line) between the values for $x=0$ and $x=1$.

substrate. Then the value of s_a can be derived from the equation

$$\sin\left(\frac{b\omega}{s_0}\right)\cos\left(\frac{a\omega}{s_a}\right) + \frac{Z_a}{Z_0}\sin\left(\frac{a\omega}{s_a}\right)\cos\left(\frac{b\omega}{s_0}\right) = 0, \quad (1)$$

where $\omega = 2\pi f_m$, and a and b are the thicknesses of the alloy layer and c-GaN buffer respectively, $s_0 = 7000$ m s^{-1} sound velocity in c-GaN [14,15], $Z_a = s_a\rho_a$ and $Z_0 = s_0\rho_0$ are acoustic impedances of the alloy and c-GaN respectively (ρ_a and ρ_0 are corresponding densities). The densities of the alloys are estimated by linear interpolation of the values for c-GaN and c-AlN [20]: $\rho_a = (6000 - 2800x)$ kg m^{-3}. The corresponding values of ρ_a are presented in Table I. The filled symbols in the right inset of Fig. 1 show the values of s_a derived from Eq. (1). The straight line connects the values of sound velocities measured in c-GaN [14,15] and calculated for c-AlN [20]. It is seen that the values for s_a obtained from the experiment and Eq. (1) agree very well with the linear interpolation of the sound velocity dependence on the Al content x in the alloy.

C. Brillouin oscillations

For these measurements, we used the c-(AlGa)N layer attached to the substrate and excited the picosecond strain pulses in the GaAs substrate by pump beam excitation with a wavelength $\lambda_{pu} = \lambda_0/2 = 380-450$ nm from the side of the epitaxial layer. For this wavelength, the c-(AlGa)N layer is transparent, and we may also neglect the energy absorbed in the c-GaN cap which has a band gap at 3.2 eV (corresponding to 388 nm) due to its small thickness. The UV pump beam is absorbed strongly in the GaAs substrate in a near surface layer with a thickness of ∼10 nm. The result of this excitation is two strain pulses propagating in opposite z directions [19].

The compressive strain pulse $\eta_{zz}(z,t)$ injected into the c-(AlGa)N layer propagates there with velocity s_a, has a duration of several picoseconds, and may be well approximated by a Gaussian temporal profile [21]. The detection of the strain pulse is realized by using a probe light beam of wavelength $\lambda_{pr} = \lambda_0/3 = 250-300$ nm and measuring the changes of the light intensity reflected from the (AlGa)N layer, $\Delta R(t)$.

There are two mechanisms which govern the probe signal $\Delta R(t)$: the displacement of the interfaces in the layered structure and the photoelastic effect [22]. Both mechanisms are described by the modulation of the interference terms for the probe beams reflected at the interfaces and perturbations of the complex refractive index $n^* = n + i\kappa$ due to the photoelastic effect. The interference of the probe beam reflected from the propagating strain pulse with other reflections results in a harmonic modulation of the $\Delta R(t)$ with a frequency f_B [23]. The corresponding temporal oscillations in $\Delta R(t)$ are often called Brillouin oscillations, and for $\kappa \ll n$:

$$f_B = \frac{2s_a}{\lambda_{pr}}\sqrt{n^2 - \sin^2\theta}, \quad (2)$$

where $\theta = 30°$ is the incidence angle of the probe beam in our setup. The amplitude and the phase of the oscillations in $\Delta R(t)$ depend on the complex photoelastic constant which depends on λ_{pr}. In our experiments we observe Brillouin oscillations for all three studied alloys, and the corresponding signals $\Delta R(t)$ are shown in the (a) panels of Figs. 2–4 for the alloys with
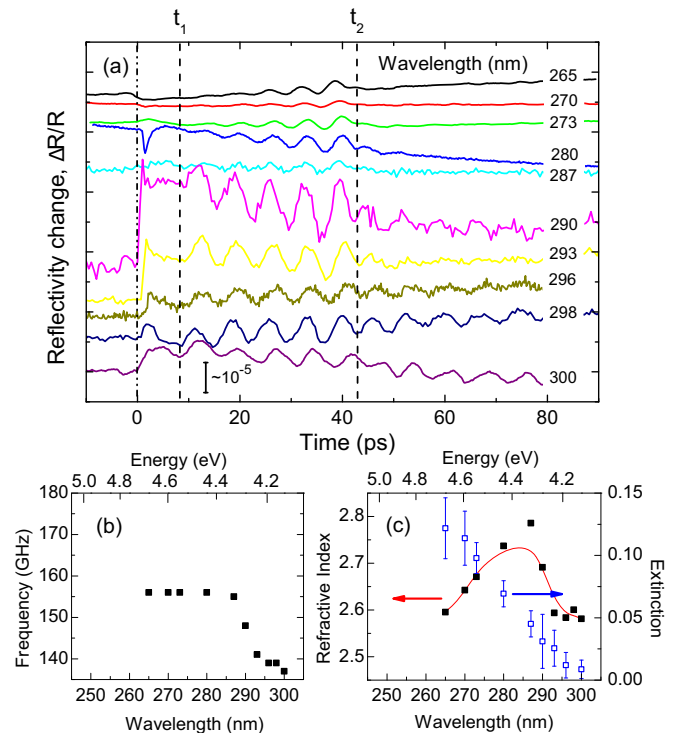

FIG. 2. Results of pump-probe experiment with picosecond strain pulses generated in GaAs substrate and injected into the c-Al$_x$Ga$_{1-x}$N alloy with $x = 0.42$: (a) measured pump-probe signals $\Delta R(t)$ for various probe wavelength; vertical dashed lines t_1 and t_2 correspond to the temporal moments when the strain pulse enters the GaN/AlGaN and open surface interfaces respectively; (b) the dependence of the frequency f_B of the Brillouin oscillations on the probe wavelength; (c) the dependence of real (closed squares) and imaginary (open squares) parts of the complex refractive index in the alloy layer on the probe wavelength; the red solid line in (c) corresponds to the smoothed on five experimental points curve.

$x = 0.42$, 0.49, and 0.66 respectively. Vertical dashed-dotted lines at $t = 0$ correspond to the time when the pump pulse excites the GaAs substrate. Vertical dashed lines at $t_1 \approx 10$ ps and $t_2 \approx 40$ ps correspond to moments when the picosecond strain pulse enters the alloy layer after passing the c-GaN buffer and hits the free surface of the alloy respectively. The positions of t_1 and t_2 depend on the exact sample in accordance with the thicknesses of the buffer and alloy layers. The frequencies f_B are derived from performing the FFT of the oscillations in a time window between t_1 and t_2 when the strain pulse propagates along the alloy layer towards the free surface. The FFT is performed after subtracting a slow varying background of $\Delta R(t)$. The FFT spectrum of the oscillations is a single line with a shape that is close to symmetric which allows us to determine f_B as the central frequency of the spectral profile with an accuracy ∼1%. The corresponding dependencies of f_B on λ_{pr} are shown in panel (b) of Figs. 2–4.

The spatial width of the strain pulse in our experiment is ∼10 nm which is much less than the thickness of the alloy layer ∼300 nm. Thus the contribution from interface displacement to the probe signal should take place only in the intervals ∼2 ps near the times t_1 and t_2 marked by vertical dashed lines in Figs. 2–4 while the major part of the temporal interval
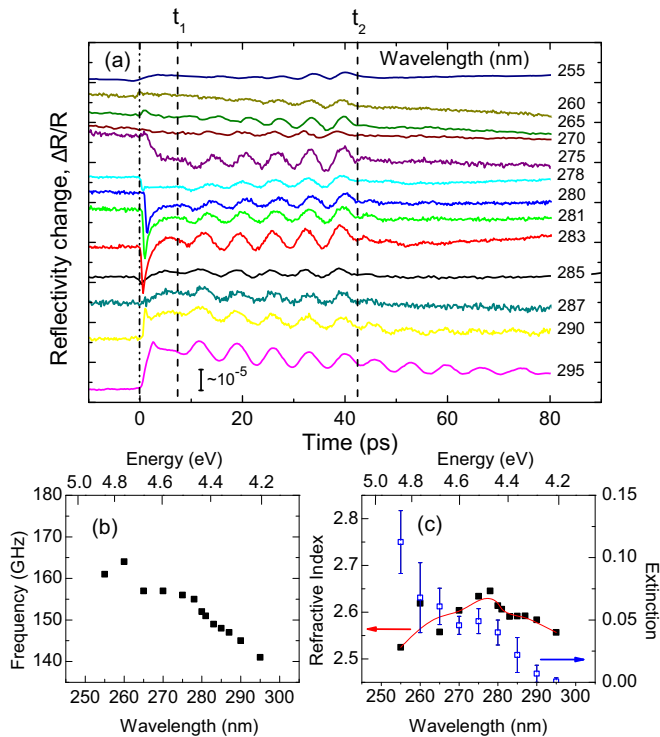
FIG. 3. Results of pump-probe experiment with picosecond strain pulses generated in GaAs substrate and injected into the c-Al$_x$Ga$_{1-x}$N alloy with $x = 0.49$: (a) measured pump-probe signals $\Delta R(t)$ for various probe wavelength; vertical dashed lines t_1 and t_2 correspond to the temporal moments when the strain pulse enters the GaN/AlGaN and open surface interfaces respectively; (b) the dependence of the frequency f_B of the Brillouin oscillations on the probe wavelength; (c) the dependence of real (closed squares) and imaginary (open squares) parts of the complex refractive index in the alloy layer on the probe wavelength; the red solid line in (c) corresponds to the smoothed on five experimental points curve.

FIG. 4. Results of pump-probe experiment with picosecond strain pulses generated in GaAs substrate and injected into the c-Al$_x$Ga$_{1-x}$N alloy with $x = 0.66$: (a) measured pump-probe signals $\Delta R(t)$ for various probe wavelength; vertical dashed lines t_1 and t_2 correspond to the temporal moments when the strain pulse enters the GaN/AlGaN and open surface interfaces respectively; (b) the dependence of the frequency f_B of the Brillouin oscillations on the probe wavelength; (c) the dependence of real (closed squares) and imaginary (open squares) parts of the complex refractive index in the alloy layer on the probe wavelength; the red solid line in (c) corresponds to the smoothed on five experimental points curve.

$t_1 - t_2$ includes only photoelastic effect. Moreover, we do not see high-amplitude spikes at t_1 and t_2 which suggests a relatively weak contribution from the displacement effect. Therefore in the analysis of the results we consider only the photoelastic effect.

The values of refractive indices n are calculated using Eq. (2) and shown in panels (c) of Figs. 2–4. The solid lines are the result of smoothing out adjacent points. The accuracy of obtaining n is approximately 5% and is dependent on the error in our estimation of the sound velocity s_a (see Table I). The extinction coefficients κ, calculated from the dependencies of the amplitude of the oscillations on time, are shown also in panel (c) of Figs. 2–4 together with n.

Qualitatively the $\Delta R(t)$ signals measured at $\lambda_{pr} < 280$ nm for all three studied layers are similar: all of them possess harmonic oscillations. However, their amplitude and dependencies on λ_{pr} are different. The existence, or alternatively the absence, of Brillouin oscillations after the reflection of the strain pulse from the free surface (corresponding to the time $t > t_2$) depends on the reflection of coherent phonons with f_B from the surface. The, ideally flat, surface plays the role of a perfect mirror for phonons and Brillouin oscillations with the same amplitude are observed immediately before
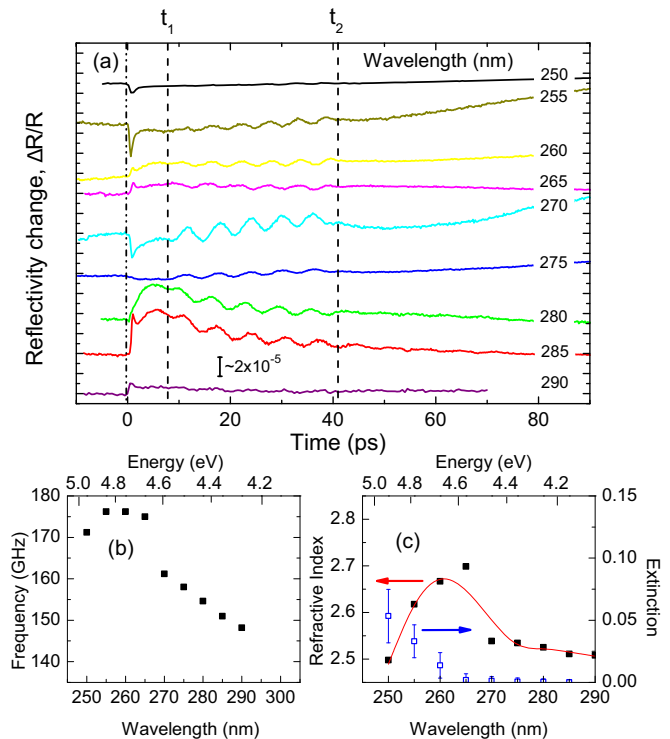
and after reflection, as seen in the lower curve in Fig. 2(a) ($x = 0.42$ and $\lambda_{pr} = 300$ nm). Alternatively, phonons with wavelength comparable with the scale of the surface roughness are strongly scattered at the surface, and the amplitude of Brillouin oscillations immediately after the reflection of the strain pulse is much lower than immediately before reflection.

III. ANALYSIS AND DISCUSSION

We begin with the discussion of the measured complex refractive index and its comparison with the data obtained from ellipsometry experiments. Then, we will turn to the discussion of the photoelastic effect, which defines the amplitude and sign of the Brillouin oscillations. Finally, we shall discuss the reflection of phonons from the free surface.

A. Complex refractive index

The dependence of n on the probe wavelength, panel (c) in Figs. 2–4, possesses a maximum at photon energy E_0, which is typical for the refractive index of GaN and their alloys for photon energies near the fundamental band gap E_g [6,7]. The width of the maximum in the studied alloys is around 20 nm
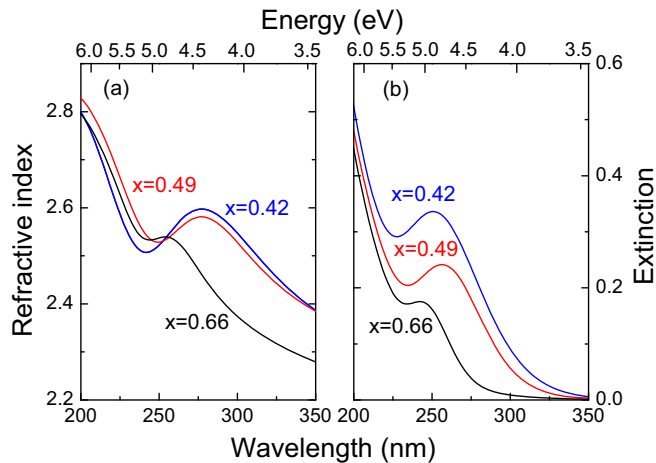
FIG. 5. The photon energy dependencies of (a) refractive indices n and (b) extinction coefficients κ obtained from ellipsometry measurements for the samples with various x.

($\sim$300 meV) which is typical for cubic nitride alloys [6,7]. The extinction coefficient κ shows a decrease with increasing wavelength which is also typical for semiconductors in the region close to the direct band gap. We associate the peak position in the wavelength dependence of n with the onset for optical electron-hole transition and correspondingly with the band gap E_g of the alloy (i.e., $E_g = E_0$). As was shown in previous studies with c-GaN [24], c-AlN [25], and (AlGa)N alloys [8] this is a good approximation and the values of E_g defined in such a way are presented in Table I. We do not see any experimental evidence of indirect band gap in (AlGa)N which could happen when x approaches the value of 0.7 [8]. However, this fact does not exclude the existence of an indirect band gap around 5 eV. A more definite conclusion requires detailed studies which are beyond the scope of the present work where we aim at photoelastic effects.

Table I shows also the values of n, κ, and correspondingly E_g measured by ellipsometry in this work [18]. The ellipsometry data for three samples are shown in Fig. 5. Comparing picosecond ultrasonic and ellipsometry measurements (cf. the values in Table I) we see that both techniques show the peaks in the wavelength dependence of n. The values of n at the peak, the position of the peaks, and correspondingly the value of $E_g = E_0$ are quite close to the values measured using picosecond ultrasonics. A more significant difference is observed for the extinction coefficients κ: the values of κ measured by ellipsometry are, in general, higher as compared to the values obtained from picosecond ultrasonics. This difference may be due to additional contributions from phonon scattering on the defects and inhomogeneities in the alloys [26,27]. Phonon scattering will result in the decrease of the amplitude of the oscillations with time while the strain pulse is propagating in (AlGa)N layer from the GaAs substrate towards the free surface. Having neglected the effects of phonon scattering may explain the consistent underestimate for the value of κ obtained from picosecond acoustic experiments.

We may compare the values of n, κ, and E_g obtained by ellipsometry in the present work with the values reported earlier [6–8]. There is quite a big difference in n and E_g

between our data and values measured in [6,7], but the values for κ measured by ellipsometry are quite similar. The values of E_g measured in [8] are much closer to our data. We note that there is also a difference for c-AlN measured in [6,7] and more recent works on c-AlN [25] and (AlGa)N alloys [8]. The differences of our ellipsometry data with values obtained in earlier works [6,7] could possibly be related to different quality of the grown material, the accuracy of defining x, different substrates, and the models used in the ellipsometric analysis.

The general reason for the difference of picosecond ultrasonic and ellipsometry techniques for obtaining n, κ, and E_g could be that ellipsometry data analysis uses smooth functions to model the spectroscopic response while picosecond ultrasonics directly measures the response at particular photon energies without any fitting functions as used for model calculations in ellipsometry. Another point is that ellipsometry software uses a parameter related to surface roughness. This parameter is only a good measure for roughness on a lateral length scale that is much shorter than the wavelength of the light, i.e., 100 nm. In Sec. III C we show that this is not the case for our films.

B. Photoelastic effect

Now we turn to the analysis of the photoelastic effect which gives the dominant contribution to the measured signal $\Delta R(t)$. Brillouin oscillations, which are observed in our work in the time interval $t_1 < t < t_2$ when the strain pulse is traveling in the (AlGa)N layer, are due only to the photoelastic effect in the alloy. In picosecond ultrasonics, the changes ΔR in the reflectivity are described by the changes Δn^* of the complex refractive index n^* in the presence of dynamical strain η [9,19,22]. In direct band gap semiconductors, the biggest photoelastic response takes place for the photon energy $E = hc/\lambda$ close to the band gap E_g. For energies far from E_g the photoelastic effect is much smaller, and $|\Delta n^*/n^*|$ does not depend strongly on λ. In our case, when $\Delta R(t)$ strongly depends on λ, we shall consider only the case when dynamical strain induces the modulation of E_g. For $\eta \ll 1$ we have [16]

$$\Delta n^* = \left(\frac{dn(E)}{dE} + i \frac{d\kappa(E)}{dE} \right) \frac{dE_g}{d\eta} \eta = p\eta, \qquad (3)$$

where p is photoelastic coefficient and $dE_g/d\eta$ is known as the deformation potential and for direct band gap has a value ~ -10 eV [28]. The sign and, correspondingly, the phase of $\Delta R(t)$ depends on the optical wavelength λ. For our spectral range with a peak in n at $E = E_g$, dn/dE is positive for $E < E_g$ and alternatively dn/dE is negative for $E > E_g$. The imaginary part $d\kappa/dE$ is always positive. The obtained wavelength dependencies of n and κ shown in panel (c) of Figs. 2–4 and Eq. (2) gives an estimate of the real and imaginary contributions to $\Delta n^* = (\alpha + i\beta)\eta$. The dimensionless constants α and β are associated with photoelastic parameters p and their values Eq. (2) are shown in Table I, obviously $\alpha = 0$ at $E = E_g$. The accuracy for the values of photoelastic constants is limited by the accuracy of deformation potential whose value is not precisely known for the c-AlGaN alloys. From [28] and references therein we may estimate the uncertainty of defining photoelastic constants to be $\sim 20\%$ and so in the interest of

prudence we present only the first significant digit for α and β in Table I. The quantitative calculation of the reflectivity changes $\Delta R(t)/R_0$ (R_0: reflectivity at $\eta = 0$) can be performed on the basis of analytical [19,22] or numerical [16] approaches. We estimate the maximum amplitude of the Brillouin oscillations using the equations for $\Delta R(t)/R_0$ derived in [19]. For short strain pulse and $\kappa \ll n$ we get

$$\frac{\Delta R(t)}{R_0} \approx \frac{16\pi n p \eta \Delta z}{\lambda (n^2 - 1)}, \tag{4}$$

where $\Delta z \sim 10$ nm is the spatial length of the strain pulse. For $p \sim 10$ the estimate gives $\Delta R(t)/R_0 \sim 10\eta$ that is consistent with the experimental value $|\Delta R(t)|/R_0 \sim 10^{-4}$ for the strain amplitude $\eta \sim 10^{-5}$. This strain amplitude is a reasonable value for the pump excitation density $\sim 10\,\mu\text{J/cm}^2$ in the GaAs substrate used in our experiments. The obtained values between 1 and 10 for α and β (see Table I) are of the same order of magnitude as for other direct band gap semiconductors for light with photon energy $E \sim E_g$. For instance, for GaAs ($E_g = 1.43$ eV) $\alpha = 2.8$ and $\beta = 2.6$ for photon energy $E = 1.65$ eV [29,30]. For the semiconductors with a sharp dielectric function near E_g the values of α and β may be quite high when E approaches E_g from the low energy side. For instance, using the data obtained in [24] for dielectric function in c-GaN ($E_g = 3.23$ eV) and deformation potential 10 eV we get $\alpha \approx 10$ and $\beta \approx 20$.

The analysis of the phase of the Brillouin oscillations in the studied samples requires the inclusion of the imaginary parts of n^* and Δn^*. We perform a qualitative analysis of the phase dynamics in the signals $\Delta R(t)/R_0$ presented in Fig. 4(a) for the alloy with $x = 0.66$. It is seen that $\Delta R(t)/R_0$ undergoes a π phase change between $\lambda_{pr} = 265$ and 270 nm. This phase change takes place when the photon energy $E \approx E_g$ where $|\Delta n^*| \approx 0$. This example shows how the photoelastic effect may be used for accurate measurements of the band gap in the nitride alloys even if the dependence of n on λ is not known.

C. Surface roughness

The fact that for most of the used λ_{pr} the Brillouin oscillations are observed only for $t_1 < t < t_2 < 40$ps [see panel (a) of Figs. 2–4] indicates a strong scattering of the corresponding phonons at the free surface. There are only a few signals measured at long wavelengths, $\lambda_{pr} > 290$ nm, for the samples with $x = 0.42$ and 0.49 when the oscillations are detected after the reflection of the strain pulse at the free surface. Obviously, the scattering at the surface increases with the increase of phonon frequency f_B of the Brillouin oscillations. The experimental results show that in all studied samples strong scattering starts at a frequency $f_s \approx 150$ GHz, which corresponds to a phonon wavelength, $\Lambda_s = c/f_s$, of about 50 nm. If the rms surface roughness R_{rms} is of the order of, or larger than, $\Lambda_s/4$, in the area of the probe spot ($\sim 20\,\mu$m in our experiments), the coherence will be lost in the reflected phonon flux and Brillouin oscillations will not be detected. From our picosecond ultrasonic data we estimate that $R_{\text{rms}} \sim 10$ nm.

We have measured the surface roughness independently using atomic force microscopy (AFM). In a $5\,\mu\text{m} \times 5\,\mu\text{m}$ square, R_{rms} is found to be (in nm) 7 ± 3, 30 ± 14, and 20 ± 4
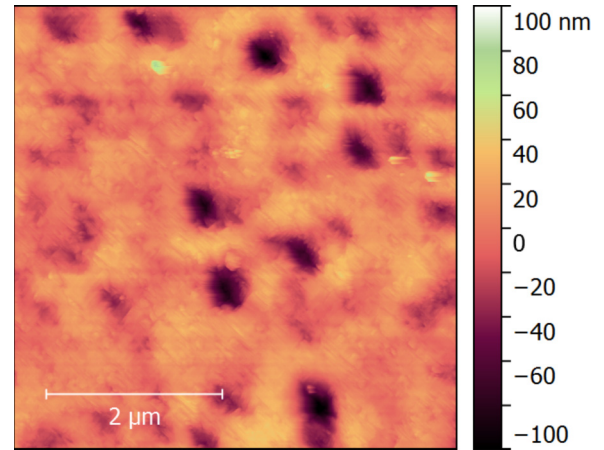

FIG. 6. AFM image measured on the surface of the $Al_xGa_{1-x}N$ film $x = 0.49$. 2 μm scale bar is shown.

for films with $x = 0.42$, 0.49, and 0.66 respectively. The AFM image for the sample with $x = 0.49$ is shown in Fig. 6. The values obtained by AFM are in reasonable agreement with the values estimated from picosecond acoustics. The deviations in height take place with a lateral correlation length of $\sim 1\,\mu$m which is smaller than the diameter of the picosecond probe spot. However, this lateral scale is larger than the visible and UV probe wavelengths used in ellipsometry, which means that the assumptions of the effective medium approximation are not satisfied and so standard ellipsometric analysis cannot make an accurate estimate of the surface roughness (see Sec. III A). Comparing the picosecond ultrasonic data to the AFM data demonstrates the possibility of measuring the surface roughness in the nitride alloys using the picosecond ultrasonic technique.

IV. CONCLUSIONS

We have used picosecond ultrasonics for studies of the optical properties of nitride epitaxial layers in the UV spectral range. We have studied zinc-blende (i.e., cubic) (AlGa)N alloys grown by MBE on (001) GaAs substrates and measured the values of complex refractive index and their dependence on Al content and the optical wavelength in the range 250–300 nm. The real part of the refractive index possesses maximum at a wavelength close to the onset of optical transitions and correspondingly to the fundamental band gap. The velocities for longitudinal sound in the alloys have been measured from pump-probe experiments with (AlGa)N membranes. The alloy layers show a strong photoelastic effect for optical wavelengths close to the band gap which results in observation of Brillouin oscillations with frequency ~ 100 GHz. The photoelastic parameters of the alloys have been derived from the analysis of Brillouin oscillations on the basis of the deformation potential mechanism of the photoelastic effect. Finally, the analysis of the reflection of coherent phonons from the free surface of the alloy layer provide an estimate of the surface roughness of the material. The results are compared with the data obtained by ellipsometry and AFM.

The presented results demonstrate that picosecond ultrasonics is a powerful technique for obtaining the fundamental

properties of the materials in the UV where the usage of standard optical techniques, like ellipsometry, meets certain difficulties such as scattering of light at the surface and uncertainty in how to model optical parameters of the new materials. The photoelastic effect resulting in Brillouin oscillations of a probe beam could be exploited for ultrafast (subterahertz) modulation of UV laser beams.

[1] S. Parsons, *Advanced Oxidation Processes for Water and Wastewater Treatment* (IWA, London, 2004).

[2] M. N. Chong, B. Jin, C. W. K. Chow, and C. Saint, Recent developments in photocatalytic water treatment technology: A review, Water Res. **44**, 2997 (2010).

[3] T. Bettles, Putting deep UV LEDs to work, Compd. Semicond. **17**, 37 (2011).

[4] F. Bernardini, V. Fiorentini, and D. Vanderbilt, Spontaneous polarization and piezoelectric constants of III-V nitrides, Phys. Rev. B **56**, 10024(R) (1997).

[5] S. Li, J. Schörmann, D. J. As, and K. Lischka, Room temperature green light emission from nonpolar cubic InGaN/GaN multi-quantum-wells, Appl. Phys. Lett. **90**, 071903 (2007).

[6] H. Okumura, T. Koizumi, Y. Ishida, H. Yaguchi, and S. Yoshida, Optical characterization of cubic AlGaN epilayers by cathodoluminescence and spectroscopic ellipsometry, Phys. Status Solidi B **216**, 211 (1999).

[7] T. Suzuki, H. Yaguchi, H. Okumura, Y. Ishida, and S. Yoshida, Optical constants of cubic GaN, AlN, and AlGaN alloys, Jpn. J. Appl. Phys. **39**, L497 (2000).

[8] M. Landmann, E. Rauls, W. G. Schmidt, M. Röppischer, C. Cobet, N. Esser, T. Schupp, D. J. As, M. Feneberg, and R. Goldhahn, Transition energies and direct-indirect band gap crossing in zinc-blende $Al_xGa_{1-x}N$, Phys. Rev. B **87**, 195210 (2013).

[9] O. Matsuda, M. C. Larciprete, R. L. Voti, and O. B. Wright, Fundamentals of picosecond laser ultrasonics, Ultrasonics **56**, 3 (2015).

[10] K. H. Lin, C. M. Lai, C. C. Pan, J. I. Chyi, J. W. Shi, S. Z. Sun, C. F. Chang, and C. K. Sun, Spatial manipulation of nanoacoustic waves with nanoscale spot sizes, Nat. Nanotechnol. **2**, 704 (2007).

[11] C. Brüggemann, A. V. Akimov, A. V. Scherbakov, M. Bombeck, C. Schneider, S. Höfling, A. Forchel, D. R. Yakovlev, and M. Bayer, Laser mode feeding by shaking quantum dots in a planar microcavity, Nat. Photon. **6**, 30 (2012).

[12] T. Czerniuk, C. Brüggemann, J. Tepper, S. Brodbeck, C. Schneider, M. Kamp, S. Höfling, B. A. Glavin, D. R. Yakovlev, A. V. Akimov, and M. Bayer, Lasing from active optomechanical resonators, Nat. Commun. **5**, 4038 (2014).

[13] C. K. Sun, J. C. Liang, and X. Y. Yu, Coherent Acoustic Phonon Oscillations in Semiconductor Multiple Quantum Wells with Piezoelectric Fields, Phys. Rev. Lett. **84**, 179 (2000).

[14] D. Moss, A. V. Akimov, S. V. Novikov, R. P. Campion, C. R. Staddon, N. Zainal, C. T. Foxon, and A. J. Kent, Elasto-optical properties of zinc-blende (cubic) GaN measured by picosecond acoustics, J. Phys. D: Appl. Phys. **42**, 115412 (2009).

[15] C. He, M. Grossmann, D. Brick, M. Schubert, S. V. Novikov, C. T. Foxon, V. Gusev, A. J. Kent, and T. Dekorsy, Study of confined coherent acoustic phonon modes in a free-standing cubic GaN membrane by femtosecond spectroscopy, Appl. Phys. Lett. **107**, 112105 (2015).

[16] T. Czerniuk, T. Ehrlich, T. Wecker, D. J. As, D. R. Yakovlev, A. V. Akimov, and M. Bayer, Picosecond Acoustics in Single Quantum Wells of Cubic GaN/(AlGa)N, Phys. Rev. Appl. **7**, 014006 (2017).

[17] R. E. L. Powell, S. V. Novikov, F. Luckert, P. R. Edwards, A. V. Akimov, C. T. Foxon, R. W. Martin, and A. J. Kent, Carrier localization and related photoluminescence in cubic AlGaN epilayers, J. Appl. Phys. **110**, 063517 (2011).

[18] See Supplemental Material at http://link.aps.org/supplemental/10.1103/PhysRevMaterials.2.034606 for a schematic of the experimental setup and a detailed discussion of the modelling parameters used for ellipsometry measurements.

[19] C. Thomsen, H. T. Grahn, H. J. Maris, and J. Tauc, Surface generation and detection of phonons by picosecond light pulses, Phys. Rev. B **34**, 4129 (1986).

[20] A. F. Wright, Elastic properties of zinc-blende and wurtzite AlN, GaN, and InN, J. Appl. Phys. **82**, 2833 (1997).

[21] E. Péronne, N. Chuecos, L. Thevenard, and B. Perrin, Acoustic solitons: A robust tool to investigate the generation and detection of ultrafast acoustic waves, Phys. Rev. B **95**, 064306 (2017).

[22] O. Matsuda, O. B. Wright, D. H. Hurley, V. Gusev, and K. Shimizu, Coherent shear phonon generation and detection with picosecond laser acoustics, Phys. Rev. B **77**, 224110 (2008).

[23] C. Thomsen, H. T. Grahn, H. J. Maris, and J. Tauc, Picosecond interferometric technique for study of phonons in the Brillouin frequency range, Opt. Commun. **60**, 55 (1986).

[24] M. Feneberg, M. Röppischer, C. Cobet, N. Esser, J. Schörmann, T. Schupp, D. J. As, F. Hörich, J. Bläsing, A. Krost, and R. Goldhahn, Optical properties of cubic GaN from 1 to 20 eV, Phys. Rev. B **85**, 155207 (2012).

[25] M. Röppischer, R. Goldhahn, G. Rossbach, P. Schley, C. Cobet, N. Esser, T. Schupp, K. Lischka, and D. J. As, Dielectric function of zinc-blende AlN from 1 to 20 eV: Band gap and van Hove singularities, J. Appl. Phys. **106**, 076104 (2009).

[26] A. M. Lomonosov, A. Ayouch, P. Ruello, G. Vaudel, M. R. Baklanov, P. Verdonck, L. Zhao, and V. E. Gusev, Nanoscale noncontact subsurface investigations of mechanical and optical properties of nanoporous low-*k* material thin film, ACS Nano **6**, 1410 (2012).

[27] A. Steigerwald, Y. Xu, J. Qi, J. Gregory, X. Liu, J. K. Furdyna, K. Varga, A. B. Hmelo, G. Lüpke, L. C. Feldman, and N. Tolk,

Semiconductor point defect concentration profiles measured using coherent acoustic phonon waves, Appl. Phys. Lett. **94**, 111910 (2009).

[28] R. Riane, A. Zaoui, S. F. Matar, and A. Abdiche, Pressure dependence of electronic and optical properties of zinc-blende GaN, BN and their $B_{0.25}Ga_{0.75}N$ alloy, Physica B **405**, 985 (2010).

[29] P. Etchegoin, J. Kircher, M. Cardona, C. Grein, and E. Bustarret, Piezo-optics of GaAs, Phys. Rev. B **46**, 15139 (1992).

[30] O. B. Wright, B. Perrin, O Matsuda, and V. E. Gusev, Ultrafast carrier diffusion in GaAs probed with picosecond acoustic pulses, Phys. Rev. B **64**, 081202 (2001).